Effect of oxygen on produced hydrocarbons and hydrogen from CO_2 reduction photocatalytic process

Jianghong Wang [a], Yujie Wang [a], Ying Li [a], Yan Sun [a], Yanan Song [a], Guijie An [a], Xinyong Zhao [a,*], Yan Cao [b]

[a] Zhengzhou University of Industrial Technology, Henan 451100, China
[b] Xi'an Technological University, Xi'an 710021, China

ARTICLE INFO

ABSTRACT

A possible approach to addressing the challenges of energy scarcity and the effects of global warming through the decrease of greenhouse gases is the manufacture of hydrocarbons, particularly fuel from the photoreduction of CO_2. Here, the determination of activity/selectivity of produced hydrocarbons, hydrogen, and oxygen in the gas phase was demonstrated in the absence and presence of O_2 in an aqueous slurry on TiO_2. The conversion increases with reaction time up to the first hour but then begins to become unchanged in the presence of oxygen, suggesting catalyst deactivation. In contrast, the reaction rate and CO_2 conversion increased over 4 h when there was no oxygen, demonstrating that oxygen can be the cause of TiO_2 deactivation. Intriguingly, light-induced O_2 uptake rather than evolution was seen during optical oxygen detection investigations in photoreactions with a peak region of O_2/CO_2. H_2 production is suppressed by the presence of oxygen. Additionally, the sudden increase in hydrogen generation when oxygen is absent demonstrated that oxygen consumption and hydrogen production are taking place at the reduction site. The availability of oxygen reduced hydrocarbon productivity and H_2 production.

1. Introduction

Anthropogenic activities cause an approximate global warming of ca. 1.0 °C beyond pre-industrial stages (IPCC, 2018). This global warming is anticipated to reach 1.5 °C from 2030 to 2052 if it keeps on enhancing at the present rate without the implementation of mitigation strategies (IPCC, 2018). This global warming is attributed to the increase in greenhouse gas emissions, which without simultaneous uptake by nature, has resulted in a rise in the concentration of these gases in the atmosphere (particularly CO_2 which accounts for 60 % of global warming) (Khan & Tahir, 2019).

Fossil fuels have been a major cause of anthropogenic CO_2 production over the years. In 2020, approximately 83.2 % of global energy demands were met by fossil fuels, although renewable energy sources reported 12.5 % of these demands (BP Energy outlook, 2021). The need for developing alternative sources of energy to cater to the increased energy needs of the world has thus become increasingly apparent, as global energy demands are projected to increase to approximately 30 TW by the year 2050 in a business-as-usual model (BP Energy, 2020; Lingampalli et al., 2017).

The linear molecule's strong thermodynamic stability as well as the kinetic inertness of CO_2 lead to the low CO2 conversion efficiency in a reaction system (Li et al., 2021; Wei et al., 2018). In comparison to C–H (approximately 430 kJ mol^{-1}) and C–C (about 336 kJ mol^{-1}) bonds, the C=O bond in the CO_2 molecule has a dissociation energy of roughly 750 kJ mol^{-1} (Li et al., 2021; Wei et al., 2018). Moreover, it has a relatively poor water solubility (about 30 mM at room temperature and pressure of 1 atm). Activation and conversion of CO_2 are therefore extremely difficult (Li et al., 2021; Wei et al., 2018). In order to sort out these issues the photo-catalytic reduction of carbon dioxide to hydrocarbons may be a promising route to convert the greenhouse gas CO_2 to useful products and limit the direct emission of CO_2.

There are four main stages involved in the entire photocatalytic CO_2 reduction reaction: (i) a semiconductor absorbing light to form electron-hole pairs, (ii) separating and transferring electron-hole pairs to the semiconductor surface, (iii) surface processes for oxidizing H_2O, and (iv) surface reactions for reducing CO_2 (Ran et al., 2018).

Among different kinds of semiconductors, TiO_2 was used commonly

for photocatalytic CO_2 reduction in H_2O because of low cost, non-toxicity, high surface area, activity, inertness, and resistance to photo-conversion (Kreft et al., 2020; Liu & Li, 2014) (Li et al., 2016; Xiong et al., 2015). For CO_2 photo-reduction, mixed anatase/rutile is more effective than pure anatase or rutile (Li et al., 2008; Wang et al., 2012). It occurs as a result of the transfer that takes place between anatase and rutile as well as the effective charge separation caused by the establishment of a Schottky barrier (Scanlon et al., 2013; Tada et al., 2009). The results of the charge transfer mechanism, however, are not definitive.

It has proven possible to reduce CO_2 by photocatalysis in both the liquid (slurry) and gas phases (flow and batch) (Kreft et al., 2020). Using a flow mode in the gas phase is fairly constrained because the product concentrations are much lower than in a batch reactor (Kreft et al., 2020). A slurry reactor's drawback in the liquid phase is the requirement for a large amount of water to be present (Kreft et al., 2020). The liquid phase is typically made up of water, which serves as a crucial reagent for CO_2 but also inhibits CO_2 conversion due to rival proton reduction (Kreft et al., 2020) (Reduction: $4H^+ + 4e^- \rightarrow 2H_2$, Oxidation: $2H_2O + 4h^+ \rightarrow O_2 + 4H^+$).

Various semiconductors have been tested as oxidation photo-catalysts, but it is generally accepted that TiO_2 is the most-often-used photo-catalyst (Augugliaro et al., 2008; Augugliaro & Palmisano, 2010; Blount & Falconer, 2002; Chen et al., 2010, 2013; Du et al., 2020; Ferry & Glaze, 1998; Higashimoto et al., 2014; Imamura et al., 2013; Kitano et al., 2014; Li et al., 2011, 2018; Ma et al., 2019; Ouidri & Khalaf, 2009; Ouyang et al., 2016; Palmisano et al., 2007; Pan et al., 2013; Pradhan et al., 2020; She et al., 2018; Song et al., 2019; Tamio-lakis et al., 2015; Wang et al., 2015; Xie et al., 2014; Yurdakal et al., 2009, 2008; Zhang et al., 2017). The reasons for considering TiO_2 as the most common photo-catalyst are reliability (Augugliaro & Palmisano, 2010; Imamura et al., 2013; Ouyang et al., 2016; She et al., 2018; Song et al., 2019; Tamiolakis et al., 2015; Xie et al., 2014; Yurdakal et al., 2009), low cost (Augugliaro & Palmisano, 2010; Imamura et al., 2013; Ouyang et al., 2016; She et al., 2018; Song et al., 2019; Tamiolakis et al., 2015; Xie et al., 2014; Yurdakal et al., 2009), low toxicity (Augugliaro & Palmisano, 2010; Imamura et al., 2013; Ouyang et al., 2016; She et al., 2018; Song et al., 2019; Tamiolakis et al., 2015; Xie et al., 2014; Yurdakal et al., 2009), photo-stability under irradiation (e.g., chemical and thermal stability) (Augugliaro & Palmisano, 2010; Imamura et al., 2013; Ouyang et al., 2016; She et al., 2018; Song et al., 2019; Tamiolakis et al., 2015; Xie et al., 2014; Yurdakal et al., 2009), activating by UV-light and also by solar radiation (Yurdakal et al., 2009), prompting of reaction under ambient temperature and pressure (Ouidri & Khalaf, 2009; Xie et al., 2014), easy availability (Xie et al., 2014), strong oxidation activity (Song et al., 2019), favorable optoelectronic properties (Leong et al., 2014), high-energy conversion efficiency(Song et al., 2019), high pho-toactivity (Schneider et al., 2014), large surface areas (Song et al., 2019) and low particle density (Song et al., 2019). The P25/TiO_2 is a commercially available photocatalyst that has been used in many processes.

No studies have been found to quantify or even detect oxygen using P25/TiO_2. Dou et al. investigated the surface reconstruction of ZnO using facile light irradiation and it led to the promotion of CO_2RR to CH4 kinetic as well as O2 evolution reaction, but it was caused inhibiting of the competing HER and CO production(Dou et al., 2021). Some studies quantify hydrogen but the oxygen was not measured there or was not investigated the effect of oxygen on produced hydrogen or produced hydrocarbons (Akhter et al., 2015; Fang et al., 2015; Galli et al., 2017; Li et al., 2016; Liu et al., 2015; Qamar et al., 2016; Reli et al., 2017; Tahir & Tahir, 2016; Xiong et al., 2015). N-TiO_2/CuO catalyst showed the maximum formic acid generation, about 40 times higher than pure titanium dioxide. In contrast, N-TiO_2/CeO_2/CuO showed a higher H_2 evolution, around ~6 times higher than pure TiO_2 (Ibarra-Rodriguez et al., 2022).

In this paper, the activity/selectivity of produced hydrocarbons,

oxygen and hydrogen from gas phase measurements was determined in the presence of oxygen on P25/TiO_2. A constant temperature of the reactor's contents is necessary while sampling the gas phase. The conversion increases with increasing reaction time up to the first hour of the reaction but then starts to flatten out using P25/TiO_2 in the presence of oxygen suggesting catalyst deactivation. While both reaction rate and CO_2 conversion were increasing over 4 h when there is no oxygen, showing deactivation of P25/TiO_2 can be because of oxygen. Carbon deposition as the origin of catalyst deactivation was investigated using TGA and FTIR. Surprisingly, light-induced O_2 uptake rather than evolution was seen during optical O_2 detection investigations in photoreactions with a peak area of O_2/CO_2. A Significant amount of produced hydrogen belonged to the dark conditions as CO_2 reduction is the photoinduced reaction and CO_2 reduction is more competitive than water reduction. The presence of oxygen suppresses to production of H_2. Also, when there is no oxygen, the hydrogen formation is increased abruptly which shows that oxygen consumption and hydrogen production are happening in the reduction site. Here, we show how the overall activity and selectivity of the reaction can change by oxygen.

2. Experimental

2.1. Catalyst characterization

The nanoparticles morphology in the synthesised photocatalyst was scanned by a transmission electron microscope machine (TEM) by a TECHNIA 200II operating at 200 kV. The BET surface area used in this test was defined by a Micromeritics Tri-Star II 3020 equipment (Vers. 2.00). X-ray diffraction (XRD) analysis was done by a Bruker laboratory X-ray diffractometer the phase composition of the catalysts was determined using this instrument. The analysis was run at 35 kV and 40 mA in the scan range of $20°–120°$ and a $0.043°$ interval The thermal analysis system made up of a controller, related software, and DSC-TGA was utilized to display mass loss and decomposition over a temperature range. The characteristic band of the organic compounds deposited on the catalyst during the reaction was identified using the Nicolette is10 FTIR spectrophotometer, an unique characterisation technique to the vibrational characterization of moieties within the sample. At a spectral resolution of 4 cm^{-1}, 32 scans were conducted in the 500 cm^{-1} to 4000 cm^{-1} range.

2.2. Photocatalytic CO_2 reduction

The photocatalytic selective oxidation of alcohols was performed in a 100 mL reactor. Typically, a mixture of photocatalyst (5 g/L) and 0.2 M sodium bicarbonate (NaHCO$_3$, Merk, ACS reagent, $\geq$ 99.7 %) was dissolved in 100 mL of deionized water, and then injected into the reactor. In the absence of oxygen, nitrogen was sparged for 5 min to remove all available oxygen in the reactor. The suspension was sealed with a rubber stopper and aluminum crimp seal. The sealed contents were left for 24 h to ensure a uniform start time (vapor–liquid equilibrium (VLE)) for all conducted experimental runs. The suspension was photo-irradiated under magnetic stirring using a 350 W UV lamp (230 V ULTRA-VITALUX 3). The lamp was placed at a constant distance (100 mm) from the reactor. Fresh catalysts were used at different irradiation times (0.5–4 h) to have consistency and to have VLE in the reactor. The reactor was taken out of its enclosure and placed in the dark for 2 h to terminate the reaction and ensure uniformity in sample temperature (room temperature) before product analysis. After the reaction, the catalyst was recovered by washing with anhydrous ethanol and H_2O and dried in an oven at 120 °C overnight to analyse spent catalysts. The organic products were analysed and identified by GC-FID. The chromatograph system is coupled with a Polyarc™ oxidizer-methanizer and with a flame ionization detector (FID) which allows for the analysis of inorganic molecules. GC-TCD was used to measure oxygen and hydrogen under oven temperature of 70 °C, reference flow of 15 mL min^{-1}, makeup flow

of 3 mL min^{-1}, carrier and reference gas of argon.

3. Result and discussion

3.1. Catalyst characterization

The refinement of the Powder X-ray diffraction (PXRD) pattern of the photocatalysts is given in Table 1. The crystal size of all catalysts was the same before and after the experiment. The P25/TiO$_2$ had both anatase and rutile. A small decrease in rutile weight percentage and an increase of anatase in spent P25/TiO$_2$ in the presence of oxygen have happened.

The XRD patterns of the photocatalysts before and after experiments were done and were shown the same phases without any agglomeration after the experiment. Rutile and anatase phases were available before and after experiments.

Table 2 outlines the physio-chemical characteristics and a summary of the surface area and porosity measurements for each photo-catalyst. The physio-chemical characteristics of the P25/TiO$_2$ in this study are comparable with previous studies (Nguyen & Wu, 2008; Wang et al., 2018). The P25/TiO$_2$ photocatalyst surface area was 51.3 m^2/g. Also, the pores volume and average pore diameter were 0.159 cm^3 g^{-1} and 124 Å respectively.

The results of the "Thermogravimetric analysis (TGA)" are displayed in Fig. 1. The sample's mass in relation to temperature was normalized using the sample's starting weight. At a ramp rate of 10 °C/min, the temperature of the system was raised from the temperature of the room to about 1000 °C. The differential gravimetry (DTG) profile of the catalysts was obtained after more analysis by determining the derivative of the TGA profiles, as shown in Fig. 1. Using P25/TiO$_2$, a normalized weight loss of ~4 % was noted Following the P25/TiO2 experiment, there was significantly more weight loss in the presence of oxygen than without O$_2$. The first pattern in the temperature between 25 °C and 200 °C indicates a mass reduction brought on by the release of H$_2$O/organic solvents from the precursor as well as additive combinations utilized in the synthesis process. The second stage, which occurs at a temperature of 300–500 °C, represents the decomposition of the organic residue, which caused it to deactivate more readily in the presence of oxygen than in the absence of oxygen.

FTIR spectroscopy was used to analyse the lattice vibrational behaviour of the various samples, and the results are displayed in Fig. 2. On the spent catalysts, absorption bands that were absent on the new catalyst could now be seen. It had two distinguishing bands at 1400 cm^{-1} and 1500 cm^{-1}. There were no changes in FTIR of spent P25/TiO$_2$ either during the experiment in the absence of oxygen or in the presence of oxygen.

A transmission electron microscope (TEM) was used to assess the morphology of the spent P25/TiO$_2$ after using light for 4 hrs in the presence and absence of light (Fig. 3). Lighter coating in Fig. 3A can be seen surrounding the wasted catalyst particles than Fig. 3B. This thinner layer is a sign that amorphous material is present around the catalyst particles, maybe as a result of amorphous deposits on the catalyst. On the spent catalysts, some stringy, polymeric-looking material may be visible, which could indicate that the organics that were deposited there are polymeric in nature.

Table 1

Average crystallite sizes and phase percentage of catalysts by XRD.

Parameters	Aeroxide® Degussa P25
Sample mass (g)	0.168
S$_{BET}$ BET Surface Area (m^2/g)	51.3
V$_{pore}$ Single point desorption (cm^3 g^{-1})	0.159
d$_{pore}$ Desorption average pore diameter (Å)	124

Table 2

Physio-chemical characteristics.

Catalyst	Type of phase	Phase percentage (wt%)	Crystal size L (nm)
Fresh P25	Anatase	90.5	23.5
	Rutile	9.5	51.7
Spent P25 in presence of oxygen	Anatase	89.5	25.3
	Rutile	10.5	46.5
Spent P25 in absence of oxygen	Anatase	88.7	24.8
	Rutile	11.2	50.7

3.2. O$_2$ photo-adsorption

Comparable to other TiO$_2$ photocatalysis results from the past (Author et al., 2009; Kreft et al., 2019; Liu et al., 2013), as shown in Fig. 4, we were unable to identify O$_2$ evolution in the gas phase using GC/TCD and just O$_2$ consumption happened. Quantification of the missing amounts of oxygen in the gas phase revealed that the absence of this by-product in the CO$_2$ reduction reaction could be caused by oxygen being consumed by TiO$_2$ (Dilla et al., 2019). Also, the inhibitory impact of O$_2$ on product formation in CO$_2$ reduction demonstrates that TiO$_2$ activity in this reaction depends on the consumption of this by-product (Dilla et al., 2019) or to be able to stop this by-product from being produced.

On a reduction site in the presence of oxygen, H$_2$O, CO$_2$ and O$_2$ are being reduced. Without oxygen, hydrogen formation at the reduction site increases since there is one fewer competitor there. The electrons for CO$_2$ and/or proton reduction are also provided by photooxidation of surface hydroxyl groups (Kreft et al., 2019). O$_2$ adsorption decreased sharply up to 1 hr and then decreased gradually which can be because of the rate-limiting factor of low free surface area for adsorption after 2 hrs, as shown in Fig. 4. The peak area of O$_2$/CO$_2$ in the presence of oxygen was decreased from 5.4 to 1.3 but it is in the range of 0—0.06 in the absence of oxygen.

When there is oxygen, the oxygen photo-adsorption is prior to oxygen evolution. It was tried to degas the reactor from oxygen to check the oxygen production in the oxidation site from water, as shown in Fig. 4. Thus, the low oxygen evolution indicated just from 30 mins to 1 hr that either photogenerated O$_2$ species stay adsorbed on the surface of synthesised photocatalyst and/or that another oxidation process is kinetically more favourable (Daskalaki et al., 2011). No studies have been found to detect or even quantify the oxygen using either TiO$_2$. Xiong et. al., 2015 and 2017 compared the oxygen yields during the photocatalytic reaction and stoichiometric calculation based on the seen products which were a little less than the average production rate of oxygen, demonstrating that hydrogen, methane and CO were the major products of Pt^{2+}Pt^0/TiO$_2^{-3}$ and Pt-Cu$_2$O/TiO$_2$ (Xiong et al., 2015)(Xiong et al., 2017). In the other studies, the amount of O$_2$ production on Pt$_4$/PC-TiO$_2$ (the weight ratios of Pt:TiO$_2$ = 4:100) was more than the calculated theoretical value via the formation amounts for methane, hydrogen, and CO (Jiao et al., 2017). Therefore, other hydrocarbon products may be theoretically made but not recognised, which is because of the possibility that they may exist on the surface of the catalyst or wall of the reactor (Jiao et al., 2017). However, in this study, there was no oxygen evolution in the oxidation site to be able to compare with hydrocarbon production in the reduction site or there was oxygen evolution but was used in the reduction site for the reverse reaction.

3.3. Oxygen effect on CO and hydrocarbon formation

Reaction rate and CO$_2$ conversion were incredibly higher when there was no oxygen using P25/TiO$_2$ in both gas phase and gas–liquid equilibrium than when there was oxygen, Fig. 5. Both reaction rate and CO$_2$ conversion were increasing because of producing CO and valuable hydrocarbons such as formic acid after 2 hrs when there is no oxygen, showing deactivation of P25/TiO$_2$ can be because of oxygen. Also, it
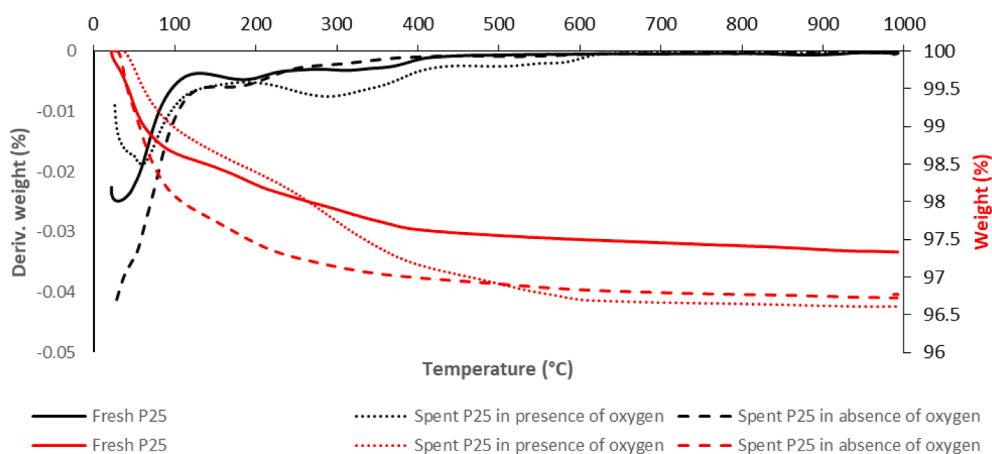
Fig. 1. Derivative (black) and weight loss (red) TGA profile of fresh (__) and spent P25 in the presence of oxygen (…) or in the absence of oxygen (− − −) during experiment.
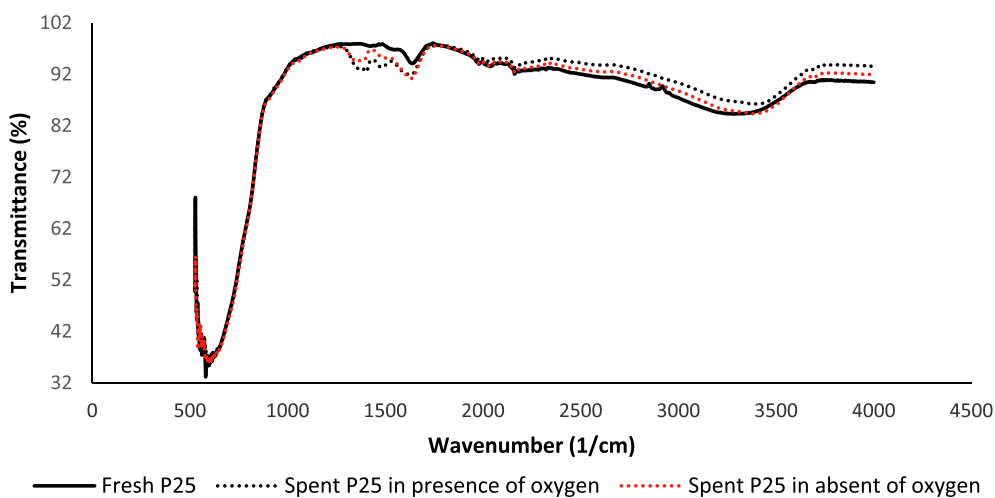
Fig. 2. FTIR spectra for the spent P25 in presence of oxygen (…), spent P25 in absent of oxygen (…), and fresh catalyst plotted as reference (__) in the range of 0–4500 cm^{-1}.
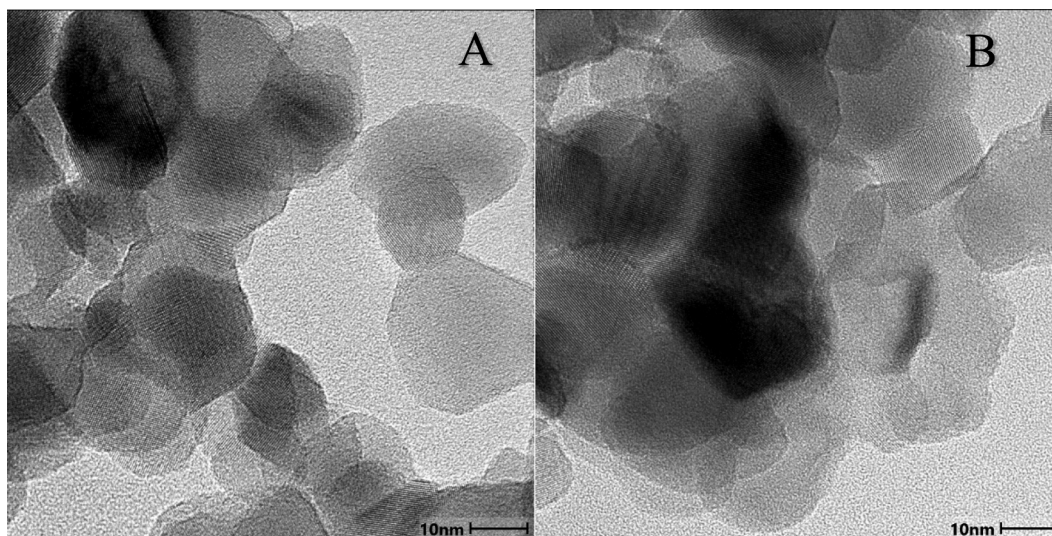
Fig. 3. TEM micrographs of A) spent P25 in absence of oxygen, B) spent P25 in presence of oxygen.
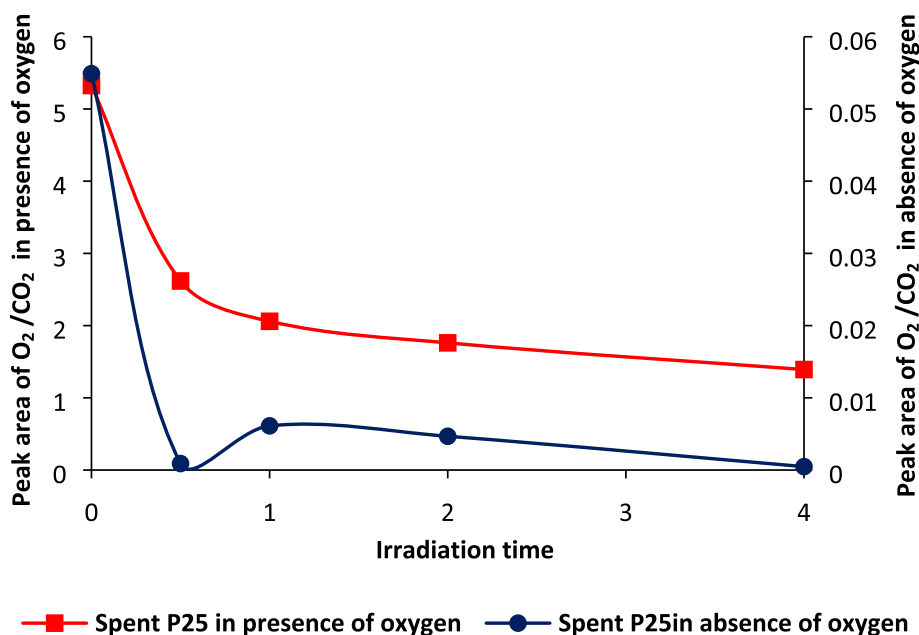
Fig. 4. Oxygen trend vs irradiation time using P25.
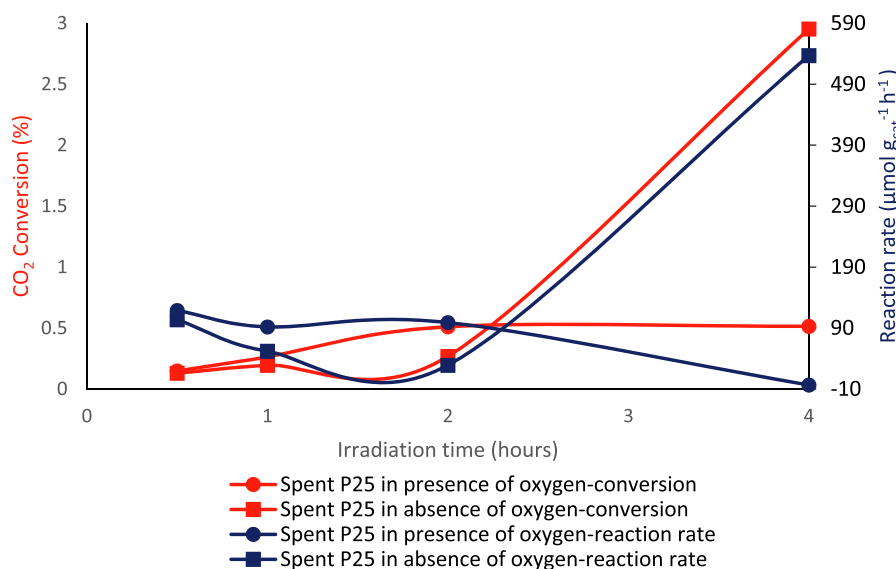
Fig. 5. CO_2 conversion and reaction rate vs irradiation time in gas phase.

showed that oxygen is a competitor for CO_2 reduction in the reduction site. The less hydrocarbon synthesis was due to the competition for charge carriers caused by the backward reaction of CO_2 reduction in the presence of highly reactive oxygen species generated on catalysts. The CO_2 conversation was increased from 0 to 0.5 % after 4 hrs in the presence of O_2 while it was observed 3 % increase in the CO_2 conversation in the absence of O_2 after 4 hrs. Also, the reaction rate was deceased with time in the presence of O_2 while it was seen a significant increase in the reaction rate in the absence of O_2 in particular in the late 2 hrs.

Beller and his co-workers, 2019 tested CO production at different oxygen percentages in CO_2 (0.1 %, 0.5 %, 5 % and 33 %) and found out whether CO would be available with or without oxygen and the highest amount of CO was investigated at 0.5 % and then 5 % (Kreft et al., 2019). Desorption of the oxygen species, which is difficult because TiO_2 has an energy advantage over CO_2 for adsorption on its surface, is a crucial

component of photocatalytic efficacy. Hence, as reaction time increases, CO_2 and O_2 fight for the same adsorption sites on TiO_2, which results in less CO_2 adsorption and less product production (Kreft et al., 2020). In this experiment, there was no methane production either in the presence or absence of oxygen as fully degassing from oxygen was so difficult. When oxygen is present, there are certain reasons not to have methane or to only have a minimal amount of it employing catalysts. Experiments on photocatalytic CO_2 reduction showed that methane synthesis is only possible in the absence of H_2 and O_2 (<5 ppm) (Dilla et al., 2019, Dilla et al., 2017). The absence of methane synthesis appears to be caused by the competition for charge carriers caused by H_2 formation and the backward reaction of CO_2 reduction caused by the presence of highly reactive oxygen species generated on catalysts (Dilla et al., 2019; Liu & Li, 2014). However, oxygen and hydrogen production during light absorption were minimal in this study (Figs. 4 and 6), and the availability of oxygen may have been the main factor.
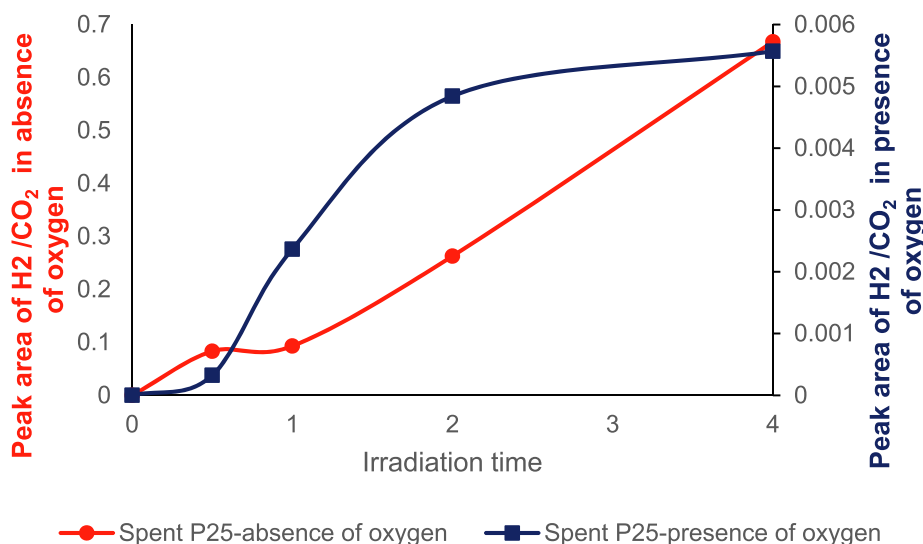
Fig. 6. Hydrogen trend vs irradiation time using P25.

3.4. H_2 formation

It has been established that the reduction of CO_2 to hydrocarbons competes with the reduction of H_2O to H_2 as was mentioned in previous studies (Jiao et al., 2017). Moreover, when oxygen is absent, hydrogen formation increases suddenly (Fig. 6), demonstrating that oxygen consumption is also the same as hydrogen production and CO_2 reduction takes place at the reduction site. The increase in H_2 is linear in the absence of oxygen and it was increased from 0 to 0.7 after 4 hrs while the hydrogen production was reached 0.0057 after 4 hrs in in the presence of oxygen. Surprisingly, in this experiment, availability of oxygen (O_2) decreased hydrocarbon productivity and H_2 creation the opposite of the result of previous research that hydrocarbon was increased (Kreft et al., 2019). Beller and his colleagues studied hydrogen generation in 2019 using 6.3-Cu/TiO2-AG, TiO2-AG, and P25/TiO2 at various oxygen percentages in CO_2 (0.1 %, 0.5 %, 5 %, and 33 %) and discovered that hydrogen would be negligible over 5 % O_2/CO_2 (Kreft et al., 2019).

On the one hand, some studies showed that the type of catalyst has an effect on CO_2 reduction but not H_2 production (Kreft et al., 2019; Liu et al., 2013; Singhal et al., 2016; Tseng et al., 2004). CO generation was three times higher when using 6.3 Cu/TiO2-AG (5.1 µmol $g_{cat}^{-1}h^{-1}$) than it was when using pristine TiO2-AG (1.5 µmol $g_{cat}^{-1}h^{-1}$); however, hydrogen evolution still predominated (430 vs 200 µmol $g_{cat}^{-1}h^{-1}$) (Kreft et al., 2019). The activity toward CO increased significantly (10.9 µmol $g_{cat}^{-1}h^{-1}$) when Cu loading was decreased to 0.3 wt%, but H_2 production was only little impacted (490 µmol $g_{cat}^{-1}h^{-1}$). More dispersion and smaller particles caused by less Cu on the surface avoid charge recombination, which encourages CO_2 photo reduction but does not affect water reduction (Kreft et al., 2019; Liu et al., 2013; Singhal et al., 2016; Tseng et al., 2004). On the other hand, some research shows the catalyst will be effective in hydrogen production. Amorphous TiO_2 can scavenge holes and greatly enhance charge carrier separation (Yu et al., 2016) and the defects in its structure can be advantageous (Ambrožová et al., 2018); increased hydrogen production from water splitting when using amorphous TiO_2 and 0.5 wt% Cu/TiO2 (Ambrožová et al., 2018) than P25/TiO_2.

4. Conclusion

The production of hydrocarbons from the photoreduction of CO_2 is one potential strategy for resolving the issues of energy scarcity and the results of global warming by reducing greenhouse gases. Here, the gas phase measurements used to determine the activity/selectivity of generated hydrocarbons, hydrogen, and oxygen were shown in the presence and absence of oxygen in an aqueous slurry on P25/TiO_2 to examine the impact of oxygen on their by-products. Up to the first hour of the reaction, the conversion goes up with reaction time, but after that, it starts to flatten out when employing spent P25 in presence of oxygen, which suggests catalyst deactivation. As evidence that oxygen can be the reason for P25/TiO_2 deactivation, the reaction rate and CO_2 conversion increased over the course of 4 h when there was no oxygen present. Intriguingly, during optical O_2 detection investigations, light-induced O_2 uptake rather than evolution was seen in photoreactions with a peak region of O_2/CO_2. The presence of oxygen inhibits the synthesis of H_2. Furthermore, the fast rise in hydrogen generation in the absence of oxygen shows that oxygen consumption, CO_2 reduction and hydrogen synthesis occur at the reduction site. Surprisingly, oxygen reduced H_2 production and hydrocarbon output. The mechanism investigation, modification of photocatalyst structure, and investigation of affinity of adsorption material play a key role in enhancing CO_2 photocatalytic reduction to produce more valuable hydrocarbons, oxygen, and hydrogen evolution. Furthermore, using XPS to address O spectra and clarification of oxygen vacancy level would be recommended in future studies.

Declaration of Competing Interest

References

Akhter, P., Hussain, M., Saracco, G., Russo, N., 2015. Novel nanostructured-TiO2 materials for the photocatalytic reduction of CO2 greenhouse gas to hydrocarbons and syngas. Fuel 149, 55–65. https://doi.org/10.1016/j.fuel.2014.09.079.

Ambrožová, N., Reli, M., Šihor, M., Kuśtrowski, P., Wu, J.C.S., Kočí, K., 2018. Copper and platinum doped titania for photocatalytic reduction of carbon dioxide. Appl. Surf. Sci. 430, 475–487. https://doi.org/10.1016/j.apsusc.2017.06.307.

Augugliaro, V., Kisch, H., Loddo, V., López-Muñoz, M.J., Márquez-Álvarez, C., Palmisano, G., Palmisano, L., Parrino, F., Yurdakal, S., 2008. Photocatalytic oxidation of aromatic alcohols to aldehydes in aqueous suspension of home-prepared titanium dioxide. 1. Selectivity enhancement by aliphatic alcohols. Appl. Catal. A Gen. 349, 182–188. https://doi.org/10.1016/j.apcata.2008.07.032.

Augugliaro, V., Palmisano, L., 2010. Green oxidation of alcohols to carbonyl compounds by heterogeneous photocatalysis. ChemSusChem 3, 1135–1138. https://doi.org/10.1002/cssc.201000156.

Author, C., Nasution, H.W., Purnama, E., Riyani, K., Gunlazuardi, J., 2009. Effect of Copper Species in a Photocatalytic Synthesis of Methanol from Carbon Dioxide over Copper-doped Titania Catalysts. World Appl. Sci. J. 6, 112–122.

Blount, M.C., Falconer, J.L., 2002. Steady-state surface species during toluene photocatalysis. Appl. Catal. B Environ. 39, 39–50. https://doi.org/10.1016/S0926-3373(01)00152-7.

BP Energy, 2020. Energy Outlook 2020 edition explores the forces shaping the global energy transition out to 2050 and the surrounding that. BP Energy Outlook 2030, Stat. Rev. London Br. Pet. 81.

BP Energy outlook, 2021. Statistical Review of World Energy globally consistent data on world energy markets . and authoritative publications in the field of energy. BP Energy Outlook 2021 70, 8–20.

Chen, Z., Xu, J., Ren, Z., He, Y., Xiao, G., 2013. High efficient photocatalytic selective oxidation of benzyl alcohol to benzaldehyde by solvothermal-synthesized ZnIn2S4 microspheres under visible light irradiation. J. Solid State Chem. 205, 134–141. https://doi.org/10.1016/j.jssc.2013.07.015.

Chen, X., Zheng, Z., Ke, X., Jaatinen, E., Xie, T., Wang, D., Guo, C., Zhao, J., Zhu, H., 2010. Supported silver nanoparticles as photocatalysts under ultraviolet and visible light irradiation. Green Chem. 12, 414–419. https://doi.org/10.1039/b921696k.

Daskalaki, V.M., Panagiotopoulou, P., Kondarides, D.I., 2011. Production of peroxide species in Pt/TiO2 suspensions under conditions of photocatalytic water splitting and glycerol photoreforming. Chem. Eng. J. 170, 433–439. https://doi.org/10.1016/j.cej.2010.11.093.

Dilla, M., Schlögl, R., Strunk, J., 2017. Photocatalytic CO2 Reduction Under Continuous Flow High-Purity Conditions: Quantitative Evaluation of CH4 Formation in the Steady-State. ChemCatChem 9, 696–704. https://doi.org/10.1002/cctc.201601218.

Dilla, M., Jakubowski, A., Ristig, S., Strunk, J., Schlögl, R., 2019. The fate of O2 in photocatalytic CO2 reduction on TiO2 under conditions of highest purity. Phys. Chem. Chem. Phys. 21, 15949–15957. https://doi.org/10.1039/c8cp07765g.

Dou, Y., Zhou, A., Yao, Y., Lim, S.Y., Li, J.R., Zhang, W., 2021. Suppressing hydrogen evolution for high selective CO2 reduction through surface-reconstructed heterojunction photocatalyst. Appl. Catal. B Environ. 286, 119876 https://doi.org/10.1016/j.apcatb.2021.119876.

Du, M., Zeng, G., Ye, C., Jin, H., Huang, J., Sun, D., Li, Q., Chen, B., Li, X., 2020. Solvent-free photo-thermocatalytic oxidation of benzyl alcohol on Pd/TiO2 (B) nanowires. Mol. Catal. 483, 110771 https://doi.org/10.1016/j.mcat.2020.110771.

Fang, B., Xing, Y., Bonakdarpour, A., Zhang, S., Wilkinson, D.P., 2015. Photodriven reduction of CO2 to CH4. ACS Sustain. Chem. Eng. 3, 2381–2388. https://doi.org/10.1021/acssuschemeng.5b00724.

Ferry, J.L., Glaze, W.H., 1998. Photocatalytic reduction of nitro organics over illuminated titanium dioxide: Role of the TiO2 surface. Langmuir 14, 3551–3555. https://doi.org/10.1021/la971079x.

Galli, F., Compagnoni, M., Vitali, D., Pirola, C., Bianchi, C.L., Villa, A., Prati, L., Rossetti, I., 2017. CO2 photoreduction at high pressure to both gas and liquid products over titanium dioxide. Appl. Catal. B Environ. 200, 386–391. https://doi.org/10.1016/j.apcatb.2016.07.038.

Higashimoto, S., Shirai, R., Osano, Y., Azuma, M., Ohue, H., Sakata, Y., Kobayashi, H., 2014. Influence of metal ions on the photocatalytic activity: Selective oxidation of benzyl alcohol on iron (III) ion-modified TiO2 using visible light. J. Catal. 311, 137–143. https://doi.org/10.1016/j.jcat.2013.11.013.

Ibarra-Rodriguez, L.I., Pantoja-Espinoza, J.C., Luévano-Hipólito, E., Garay-Rodríguez, L. F., López-Ortiz, A., Torres-Martínez, L.M., Collins-Martínez, V.H., 2022. Formic acid and hydrogen generation from the photocatalytic reduction of CO2 on visible light activated N-TiO2/CeO2/CuO composites. J. Photochem. Photobiol. 11 https://doi.org/10.1016/j.jpap.2022.100125.

Imamura, K., Tsukahara, H., Hamamichi, K., Seto, N., Hashimoto, K., Kominami, H., 2013. Simultaneous production of aromatic aldehydes and dihydrogen by photocatalytic dehydrogenation of liquid alcohols over metal-loaded titanium(IV) oxide under oxidant- and solvent-free conditions. Appl. Catal. A Gen. 450, 28–33. https://doi.org/10.1016/j.apcata.2012.09.051.

Ipcc, 2018. Global warming of 1.5°C. An IPCC Special Report on the impacts of global warming of 1.5°C above pre-industrial levels and related global greenhouse gas emission pathways, in the context of strengthening the global response to the threat of climate change. Ipcc - Sr15 2, 17–20.

Jiao, J., Wei, Y., Chi, K., Zhao, Z., Duan, A., Liu, J., Jiang, G., Wang, Y., Wang, X., Han, C., Zheng, P., 2017. Platinum Nanoparticles Supported on TiO2 Photonic Crystals as Highly Active Photocatalyst for the Reduction of CO2 in the Presence of Water. Energy Technol. 5, 877–883. https://doi.org/10.1002/ente.201600572.

Khan, A.A., Tahir, M., 2019. Recent advancements in engineering approach towards design of photo-reactors for selective photocatalytic CO2 reduction to renewable fuels. J. CO2 Util. 29, 205–239. https://doi.org/10.1016/j.jcou.2018.12.008.

Kitano, S., Tanaka, A., Hashimoto, K., Kominami, H., 2014. Selective oxidation of alcohols in aqueous suspensions of rhodium ion-modified TiO2 photocatalysts under irradiation of visible light. Phys. Chem. Chem. Phys. 16, 12554–12559. https://doi.org/10.1039/c4cp00863d.

Kreft, S., Schoch, R., Schneidewind, J., Rabeah, J., Kondratenko, E.V., Kondratenko, V. A., Junge, H., Bauer, M., Wohlrab, S., Beller, M., 2019. Improving Selectivity and Activity of CO2 Reduction Photocatalysts with Oxygen. Chem 5, 1818–1833. https://doi.org/10.1016/j.chempr.2019.04.006.

Kreft, S., Wei, D., Junge, H., Beller, M., 2020. Recent advances on TiO2-based photocatalytic CO2 reduction. EnergyChem 2. https://doi.org/10.1016/j.enchem.2020.100044.

Leong, K.H., Monash, P., Ibrahim, S., Saravanan, P., 2014. Solar photocatalytic activity of anatase TiO2 nanocrystals synthesized by non-hydrolitic sol-gel method. Sol. Energy 101, 321–332. https://doi.org/10.1016/j.solener.2014.01.006.

Li, S., Cai, J., Wu, X., Liu, B., Chen, Q., Li, Y., Zheng, F., 2018. TiO 2 @Pt@CeO 2 nanocomposite as a bifunctional catalyst for enhancing photo-reduction of Cr (VI) and photo-oxidation of benzyl alcohol. J. Hazard. Mater. 346, 52–61. https://doi.org/10.1016/j.jhazmat.2017.12.001.

Li, G., Ciston, S., Saponjic, Z.V., Chen, L., Dimitrijevic, N.M., Rajh, T., Gray, K.A., 2008. Synthesizing mixed-phase tio 2 nanocomposites using a hydrothermal method for photo-oxidation and photoreduction applications. J. Catal. 253, 105–110. https://doi.org/10.1016/j.jcat.2007.10.014.

Li, R., Kobayashi, H., Guo, J., Fan, J., 2011. Visible-light induced high-yielding benzyl alcohol-to-benzaldehyde transformation over mesoporous crystalline TiO2: A self-adjustable photo-oxidation system with controllable hole-generation. J. Phys. Chem. C 115, 23408–23416. https://doi.org/10.1021/jp207259u.

Li, K., Peng, T., Ying, Z., Song, S., Zhang, J., 2016. Ag-loading on brookite TiO2 quasi nanocubes with exposed 210 and 001 facets: Activity and selectivity of CO2 photoreduction to CO/CH4. Appl. Catal. B Environ. 180, 130–138. https://doi.org/10.1016/j.apcatb.2015.06.022.

Li, K., Teng, C., Wang, S., Min, Q., 2021. Recent Advances in TiO2-Based Heterojunctions for Photocatalytic CO2 Reduction With Water Oxidation: A Review. Front. Chem. 9, 1–25. https://doi.org/10.3389/fchem.2021.637501.

Lingampalli, S.R., Ayyub, M.M., Rao, C.N.R., 2017. Recent progress in the photocatalytic reduction of carbon dioxide. ACS Omega 2, 2740–2748. https://doi.org/10.1021/acsomega.7b00721.

Liu, L., Gao, F., Zhao, H., Li, Y., 2013. Tailoring Cu valence and oxygen vacancy in Cu/TiO2 catalysts for enhanced CO2 photoreduction efficiency. Appl. Catal. B Environ. 134–135, 349–358. https://doi.org/10.1016/j.apcatb.2013.01.040.

Liu, L., Li, Y., 2014. Understanding the reaction mechanism of photocatalytic reduction of CO 2 with H 2 O on TiO 2 -based photocatalysts: A review. Aerosol Air Qual. Res. 14, 453–469. https://doi.org/10.4209/aaqr.2013.06.0186.

Liu, E., Qi, L., Bian, J., Chen, Y., Hu, X., Fan, J., Liu, H., Zhu, C., Wang, Q., 2015. A facile strategy to fabricate plasmonic Cu modified TiO2 nano-flower films for photocatalytic reduction of CO2 to methanol. Mater. Res. Bull. 68, 203–209. https://doi.org/10.1016/j.materresbull.2015.03.064.

Ma, J., Yu, X., Liu, X., Li, H., Hao, X., Li, J., 2019. The preparation and photocatalytic activity of Ag-Pd/g-C3N4 for the coupling reaction between benzyl alcohol and aniline. Mol. Catal. 476, 110533 https://doi.org/10.1016/j.mcat.2019.110533.

Nguyen, T., Wu, J.C.S., 2008. Photoreduction of CO 2 to fuels under sunlight using optical-fiber reactor. Sol. Energy Mater. Sol. Cells 92, 864–872. https://doi.org/10.1016/j.solmat.2008.02.010.

Ouidri, S., Khalaf, H., 2009. Synthesis of benzaldehyde from toluene by a photocatalytic oxidation using TiO2-pillared clays. J. Photochem. Photobiol. A Chem. 207, 268–273. https://doi.org/10.1016/j.jphotochem.2009.07.019.

Ouyang, W., Kuna, E., Yepez, A., Balu, A.M., Romero, A.A., Colmenares, J.C., Luque, R., 2016. Mechanochemical synthesis of TiO2 nanocomposites as photocatalysts for benzyl alcohol photo-oxidation. Nanomaterials 6, 1–12. https://doi.org/10.3390/nano6050093.

Palmisano, G., Yurdakal, S., Augugliaro, V., Loddo, V., Palmisano, L., 2007. Photocatalytic selective oxidation of 4-methoxybenzyl alcohol to aldehyde in aqueous suspension of home-prepared titanium dioxide catalyst. Adv. Synth. Catal. 349, 964–970. https://doi.org/10.1002/adsc.200600435.

Pan, X., Zhang, N., Fu, X., Xu, Y.J., 2013. Selective oxidation of benzyl alcohol over TiO2 nanosheets with exposed 0 0 1 facets: Catalyst deactivation and regeneration. Appl. Catal. A Gen. 453, 181–187. https://doi.org/10.1016/j.apcata.2012.12.023.

Pradhan, S.R., Nair, V., Giannakoudakis, D.A., Lisovytskiy, D., Colmenares, J.C., 2020. Design and development of TiO2 coated microflow reactor for photocatalytic partial oxidation of benzyl alcohol. Mol. Catal. 486, 110884 https://doi.org/10.1016/j.mcat.2020.110884.

Qamar, S., Lei, F., Liang, L., Gao, S., Liu, K., Sun, Y., Ni, W., Xie, Y., 2016. Ultrathin TiO2 flakes optimizing solar light driven CO2 reduction. Nano Energy 26, 692–698. https://doi.org/10.1016/j.nanoen.2016.06.029.

Ran, J., Jaroniec, M., Qiao, S.Z., 2018. Cocatalysts in semiconductor-based photocatalytic CO2 Reduction: achievements, challenges, and opportunities. Adv. Mater. 30, 1–31. https://doi.org/10.1002/adma.201704649.

Reli, M., Kobielusz, M., Matějová, L., Daniš, S., Macyk, W., Obalová, L., Kuśtrowski, P., Rokicińska, A., Kočí, K., 2017. TiO2 Processed by pressurized hot solvents as a novel photocatalyst for photocatalytic reduction of carbon dioxide. Appl. Surf. Sci. 391, 282–287. https://doi.org/10.1016/j.apsusc.2016.06.061.

Scanlon, D.O., Dunnill, C.W., Buckeridge, J., Shevlin, S.A., Logsdail, A.J., Woodley, S.M., Catlow, C.R.A., Powell, M.J., Palgrave, R.G., Parkin, I.P., Watson, G.W., Keal, T.W., Sherwood, P., Walsh, A., Sokol, A.A., 2013. Band alignment of rutile and anatase TiO2. Nat. Mater. 12, 798–801. https://doi.org/10.1038/nmat3697.

Schneider, J., Matsuoka, M., Takeuchi, M., Zhang, J., Horiuchi, Y., Anpo, M., Bahnemann, D.W., 2014. Understanding TiO2photocatalysis: Mechanisms and materials. Chem. Rev. 114, 9919–9986. https://doi.org/10.1021/cr5001892.

She, H., Zhou, H., Li, L., Wang, L., Huang, J., Wang, Q., 2018. Nickel-doped excess oxygen defect titanium dioxide for efficient selective photocatalytic oxidation of benzyl alcohol. ACS Sustain. Chem. Eng. 6, 11939–11948. https://doi.org/10.1021/acssuschemeng.8b02217.

Singhal, N., Ali, A., Vorontsov, A., Pendem, C., Kumar, U., 2016. Efficient approach for simultaneous CO and H2 production via photoreduction of CO2 with water over copper nanoparticles loaded TiO2. Appl. Catal. A Gen. 523, 107–117. https://doi.org/10.1016/j.apcata.2016.05.027.

Song, H., Liu, Z., Wang, Y., Zhang, N., Qu, X., Guo, K., Xiao, M., Gai, H., 2019. Template-free synthesis of hollow TiO2 nanospheres supported Pt for selective photocatalytic oxidation of benzyl alcohol to benzaldehyde. Green Energy Environ. 4, 278–286. https://doi.org/10.1016/j.gee.2018.09.001.

Tada, H., Kiyonaga, T., Naya, S.I., 2009. Rational design and applications of highly efficient reaction systems photocatalyzed by noble metal nanoparticle-loaded titanium(IV) dioxide. Chem. Soc. Rev. 38, 1849–1858. https://doi.org/10.1039/b822385h.

Tahir, M., Tahir, B., 2016. Dynamic photocatalytic reduction of CO 2 to CO in a honeycomb monolith reactor loaded with Cu and N doped TiO 2 nanocatalysts. Appl. Surf. Sci. 377, 244–252. https://doi.org/10.1016/j.apsusc.2016.03.141.

Tamiolakis, I., Lykakis, I.N., Armatas, G.S., 2015. Mesoporous CdS-sensitized TiO2 nanoparticle assemblies with enhanced photocatalytic properties: Selective aerobic oxidation of benzyl alcohols. Catal. Today 250, 180–186. https://doi.org/10.1016/j.cattod.2014.03.047.

Tseng, I.H., Wu, J.C.S., Chou, H.Y., 2004. Effects of sol-gel procedures on the photocatalysis of Cu/TiO2 in CO2 photoreduction. J. Catal. 221, 432–440. https://doi.org/10.1016/j.jcat.2003.09.002.

Wang, L., Zhang, X., Yang, L., Wang, C., Wang, H., 2015. Photocatalytic reduction of CO2 coupled with selective alcohol oxidation under ambient conditions. Catal. Sci. Technol. 5, 4800–4805. https://doi.org/10.1039/c5cy00772k.

Wang, L., Duan, S., Jin, P., She, H., Huang, J., Lei, Z., Zhang, T., Wang, Q., 2018. Anchored Cu(II) tetra(4-carboxylphenyl)porphyrin to P25 (TiO2) for efficient photocatalytic ability in CO2 reduction. Appl. Catal. B Environ. 239, 599–608. https://doi.org/10.1016/j.apcatb.2018.08.007.

Wang, P., Bai, Y., Liu, J., Fan, Z., Hu, Y., 2012. One-pot synthesis of rutile TiO 2 nanoparticle modi fi ed anatase TiO 2 nanorods toward enhanced photocatalytic reduction of CO 2 into hydrocarbon fuels 29, 185–188. 10.1016/j.catcom.2012.10.010.

Wei, L., Yu, C., Zhang, Q., Liu, H., Wang, Y., 2018. TiO2-based heterojunction photocatalysts for photocatalytic reduction of CO2 into solar fuels. J. Mater. Chem. A 6, 22411–22436. https://doi.org/10.1039/c8ta08879a.

Xie, M., Dai, X., Meng, S., Fu, X., Chen, S., 2014. Selective oxidation of aromatic alcohols to corresponding aromatic aldehydes using In2S3 microsphere catalyst under visible light irradiation. Chem. Eng. J. 245, 107–116. https://doi.org/10.1016/j.cej.2014.02.029.

Xiong, Z., Wang, H., Xu, N., Li, H., Fang, B., Zhao, Y., Zhang, J., Zheng, C., 2015. Photocatalytic reduction of CO2 on Pt2+-Pt0/TiO2 nanoparticles under UV/Vis light irradiation: A combination of Pt2+ doping and Pt nanoparticles deposition. Int. J. Hydrogen Energy 40, 10049–10062. https://doi.org/10.1016/j.ijhydene.2015.06.075.

Xiong, Z., Lei, Z., Kuang, C.C., Chen, X., Gong, B., Zhao, Y., Zhang, J., Zheng, C., Wu, J.C.S., 2017. Selective photocatalytic reduction of CO2 into CH4 over Pt-Cu2O TiO2 nanocrystals: The interaction between Pt and Cu2O cocatalysts. Appl. Catal. B Environ. 202, 695–703. https://doi.org/10.1016/j.apcatb.2016.10.001.

Yu, H., Chen, W., Wang, X., Xu, Y., Yu, J., 2016. Enhanced photocatalytic activity and photoinduced stability of Ag-based photocatalysts: The synergistic action of amorphous-Ti(IV) and Fe(III) cocatalysts. Appl. Catal. B Environ. 187, 163–170. https://doi.org/10.1016/j.apcatb.2016.01.011.

Yurdakal, S., Palmisano, G., Loddo, V., Augugliaro, V., Palmisano, L., 2008. Nanostructured rutile TiO2 for selective photocatalytic oxidation of aromatic alcohols in water. J. Am. Chem. Soc. 130, 1568–1569. https://doi.org/10.1021/ja709989e.

Yurdakal, S., Palmisano, G., Loddo, V., Alagöz, O., Augugliaro, V., Palmisano, L., 2009. Selective photocatalytic oxidation of 4-substituted aromatic alcohols in water with rutile TiO2 prepared at room temperature. Green Chem. 11, 510–516. https://doi.org/10.1039/b819862d.

Zhang, B., Li, J., Gao, Y., Chong, R., Wang, Z., Guo, L., Zhang, X., Li, C., 2017. To boost photocatalytic activity in selective oxidation of alcohols on ultrathin Bi2MoO6 nanoplates with Pt nanoparticles as cocatalyst. J. Catal. 345, 96–103. https://doi.org/10.1016/j.jcat.2016.11.023.